Splice Length of Prestressing Strand in Field-Cast UHPC Connections

February 2014

NTIS Accession No. PB2014-103454

FHWA Publication No. FHWA-HRT-14-047

U.S. Department of Transportation
Federal Highway Administration

FOREWORD

With the ever increasing congestion and deterioration of our nation's highway system, a need exists to develop highly durable and rapidly constructed infrastructure systems. Durable bridge structures that would require less intrusive maintenance and would exhibit longer life spans thus maximizing the use of the facility are highly desirable. Expediting bridge construction can minimize traffic flow disruptions. Ultra-high performance concrete (UHPC) is an advanced construction material which affords new opportunities to envision the future of the highway infrastructure. The Federal Highway Administration has been engaged in research on the optimal uses of UHPC in the highway bridge infrastructure since 2001 through its Bridge of the Future initiative. This report presents results of a study aimed at assessing the potential of using UHPC-class materials to lap splice prestressing strands in field-cast connections. This concept could potentially allow for the simplification of connection details in some prefabricated bridge systems, and may also allow for the development and deployment of expedited construction techniques.

This report corresponds to the TechBrief titled "Splice Length of Prestressing Strand in Field-Cast UHPC Connections" (FHWA-HRT-14-041). This report is being distributed through the National Technical Information Service for informational purposes. The content in this report is being distributed "as is" and may contain editorial or grammatical errors.

TECHNICAL REPORT DOCUMENTATION PAGE

1. Report No. FHWA-HRT-14-047	2. Government Accession No. NTIS PB2014-103454	3. Recipient's Catalog No.
4. Title and Subtitle Splice Length of Prestressing Strand in Field-Cast UHPC Connections		5. Report Date February 2014
		6. Performing Organization Code:
7. Author(s) Benjamin A. Graybeal		8. Performing Organization Report No.
9. Performing Organization Name and Address Office of Infrastructure Research & Development Federal Highway Administration 6300 Georgetown Pike McLean, VA 22101-2296		10. Work Unit No.
		11. Contract or Grant No.
12. Sponsoring Agency Name and Address Office of Infrastructure Research & Development Federal Highway Administration 6300 Georgetown Pike McLean, VA 22101-2296		13. Type of Report and Period Covered March 2012 – March 2013
		14. Sponsoring Agency Code HRDI-40

15. Supplementary Notes

The research discussed herein was completed by Benjamin Graybeal who leads the FHWA Structural Concrete Research Program at the Turner-Fairbank Highway Research Center. Assistance in the fabrication of test specimens was provided by laboratory support contract staff employed by Global Consulting, Inc. and working at TFHRC under contract DTFH61-07-C-00011.

16. Abstract

The development length of reinforcements embedded into ultra-high performance concrete (UHPC) can be significantly shorter than the lengths normally associated with conventional concrete. Shortening the development length of prestressing strand can allow for a redesign of some structural systems, including spliced girder and continuous-for-live-load bridges. Ultra-high performance concrete (UHPC), when used in field-cast connections between prefabricated bridge elements, can create robust connections which emulate monolithic components. This study investigated the development length of 0.5 and 0.6 inch (12.7 and 15.2 mm) diameter untensioned prestressing strands embedded in steel fiber and PVA fiber reinforced UHPC. The volumetric fiber content was 2 percent. A novel tension test method allowed for replication of the tension-tension stress state that would occur when two strands are lap spliced within a connection between two linear elements. The results suggest that, for the steel fiber reinforced UHPC, the 0.5 inch (12.7 mm) diameter strands can be fully developed within 20 inches (0.51 m) and the 0.6 inch (15.2 mm) diameter strands can be fully developed in approximately 24 inches (0.61 m). The 0.5 inch (12.7 mm) diameter strands can be fully developed in the PVA fiber reinforced UHPC in approximately 36 inches (0.91 m).

This report corresponds to the TechBrief titled "Splice Length of Prestressing Strand in Field-Cast UHPC Connections" (FHWA-HRT-14-041).

17. Key Words Ultra-high performance concrete, UHPC, fiber-reinforced concrete, prestressing strand, development length, bond stress	18. Distribution Statement No restrictions. This document is available through the National Technical Information Service, Springfield, VA 22161.

19. Security Classif. (of this report) Unclassified	20. Security Classif. (of this page) Unclassified	21. No. of Pages 38	22. Price N/A

Form DOT F 1700.7 (8-72) Reproduction of completed page authorized

SI* (MODERN METRIC) CONVERSION FACTORS

APPROXIMATE CONVERSIONS TO SI UNITS

Symbol	When You Know	Multiply By	To Find	Symbol
		LENGTH		
in	inches	25.4	millimeters	mm
ft	feet	0.305	meters	m
yd	yards	0.914	meters	m
mi	miles	1.61	kilometers	km
		AREA		
in^2	square inches	645.2	square millimeters	mm^2
ft^2	square feet	0.093	square meters	m^2
yd^2	square yard	0.836	square meters	m^2
ac	acres	0.405	hectares	ha
mi^2	square miles	2.59	square kilometers	km^2
		VOLUME		
fl oz	fluid ounces	29.57	milliliters	mL
gal	gallons	3.785	liters	L
ft^3	cubic feet	0.028	cubic meters	m^3
yd^3	cubic yards	0.765	cubic meters	m^3
	NOTE: volumes greater than 1000 L shall be shown in m^3			
		MASS		
oz	ounces	28.35	grams	g
lb	pounds	0.454	kilograms	kg
T	short tons (2000 lb)	0.907	megagrams (or "metric ton")	Mg (or "t")
		TEMPERATURE (exact degrees)		
^oF	Fahrenheit	5 (F-32)/9 or (F-32)/1.8	Celsius	^oC
		ILLUMINATION		
fc	foot-candles	10.76	lux	lx
fl	foot-Lamberts	3.426	$candela/m^2$	cd/m^2
		FORCE and PRESSURE or STRESS		
lbf	poundforce	4.45	newtons	N
lbf/in^2	poundforce per square inch	6.89	kilopascals	kPa

APPROXIMATE CONVERSIONS FROM SI UNITS

Symbol	When You Know	Multiply By	To Find	Symbol
		LENGTH		
mm	millimeters	0.039	inches	in
m	meters	3.28	feet	ft
m	meters	1.09	yards	yd
km	kilometers	0.621	miles	mi
		AREA		
mm^2	square millimeters	0.0016	square inches	in^2
m^2	square meters	10.764	square feet	ft^2
m^2	square meters	1.195	square yards	yd^2
ha	hectares	2.47	acres	ac
km^2	square kilometers	0.386	square miles	mi^2
		VOLUME		
mL	milliliters	0.034	fluid ounces	fl oz
L	liters	0.264	gallons	gal
m^3	cubic meters	35.314	cubic feet	ft^3
m^3	cubic meters	1.307	cubic yards	yd^3
		MASS		
g	grams	0.035	ounces	oz
kg	kilograms	2.202	pounds	lb
Mg (or "t")	megagrams (or "metric ton")	1.103	short tons (2000 lb)	T
		TEMPERATURE (exact degrees)		
^oC	Celsius	1.8C+32	Fahrenheit	^oF
		ILLUMINATION		
lx	lux	0.0929	foot-candles	fc
cd/m^2	$candela/m^2$	0.2919	foot-Lamberts	fl
		FORCE and PRESSURE or STRESS		
N	newtons	0.225	poundforce	lbf
kPa	kilopascals	0.145	poundforce per square inch	lbf/in^2

*SI is the symbol for the International System of Units. Appropriate rounding should be made to comply with Section 4 of ASTM E380.
(Revised March 2003)

TABLE OF CONTENTS

LIST OF FIGURES

LIST OF TABLES

CHAPTER 1. INTRODUCTION

INTRODUCTION

Highway infrastructure in the United States is aging and is sometimes incapable of adequately accommodating the volume of traffic loads. Most of the roads and bridges traveled by the public each day were designed and constructed decades ago, and these assets are in need of maintenance and rehabilitation in order to maintain an appropriate level of service. So as to keep the interruptions to the traveling public at a minimum, many transportation projects are specifying the deployment of rapid construction practices when rehabilitating existing infrastructure.

One example of this practice is known as accelerated bridge construction (ABC). One commonly deployed concept within ABC is to prefabricate significant portions of the new bridge structure offsite, then assemble and connect them onsite during an expedited construction timeframe. Precast concrete elements can provide significant benefit, as they can be designed to replace conventional cast-in-place concrete construction, thus removing critical path activities such as form construction and concrete curing from the schedule and expediting the completion of the rehabilitation.

The use of prefabricated bridge elements can necessitate the use of field-applied connections between these elements. These connections must be completed rapidly and must be sufficiently robust so as to not create a weak point within the finished structure. Field-cast concrete or other cementitious material connections have been applied countless times over recent decades. Critical aspects of these connections include the rate of mechanical property development, the dimensional stability, and the durability of the field-cast materials. These connections have frequently required complex designs, thus limiting their constructability and their use. When deployed, the connection systems have sometimes underperformed, resulting in reduced serviceability of the finished structure.

Ultra-high performance concrete (UHPC) is a relatively new class of cementitious composite materials. Research and field deployments of UHPC have demonstrated that this concrete is appropriate for use in field-cast connections between prefabricated bridge elements.[1,2] The advanced mechanical and durability properties of UHPC facilitate the design of simple connections which cease to be weak points within the finished structure.

Prestressed concrete structural elements are ubiquitous in the transportation infrastructure, with nearly every element including prestressing strands. Connecting adjacent pretensioned elements to one another affords the opportunity to increase the efficiency of the structural design and also to enhance the serviceability of the structure. Connections engaging prestressing strands extending from the components tend to be rarely used due to the need for expensive mechanical connectors or long lengths of strand (and thus geometrically large connections). Critical connections in which splicing of existing strands might have been appropriate have traditionally been completed through the use of either post-tensioning systems or supplemental mild steel reinforcement.

UHPC-class materials have been demonstrated to significantly decrease the development length of embedded reinforcing elements. As such, UHPC may afford a new opportunity to reconsider the traditional methods for connecting prestressed elements, including the splicing of prestressing strands. It may be possible to reduce the embedment length of prestressing strands to the point that splicing of pretensioned elements becomes a viable design concept and construction technique. Most notably, this concept could advance the state-of-the-practice for multi-span continuous structures and for spliced girder structures.

OBJECTIVE

The objective of this research study is to evaluate the development length of untensioned prestressing strand in steel fiber and PVA fiber reinforced UHPC formulations.

SUMMARY OF APPROACH

The research discussed herein focuses on the assessment of the development length of untensioned prestressing strand in UHPC. A novel test specimen design and associated loading apparatus was developed so as to mimic the critical tension-tension lap splice configuration that may be encountered in a field-deployed connection system. Strand development length is influenced by the confinement provided by the concrete and thus the friction between the strand and the concrete. The testing included two UHPC formulations so as to include the fiber reinforcement type and thus the higher confinement normally provided by stiffer (i.e., steel) fibers. Tests were conducted on two different diameters of prestressing strand to assess any resistance differences that may occur under the higher induced bond stresses corresponding to the higher load capacity inherent in larger strands.

OUTLINE OF REPORT

This report is divided into five chapters. Chapters 1 and 2 provide an introduction to the research and provide background information useful to understanding this study's results. Chapter 3 presents the test matrix, test setup, UHPC mixing and casting details, and the UHPC compression mechanical response. Chapter 4 presents the results of the strand development length testing. Finally, Chapter 5 presents the conclusions garnered from the results of this research.

CHAPTER 2. BACKGROUND

INTRODUCTION

The contents of this chapter include a definition of ultra-high performance concrete (UHPC) and material details specific to this class of cementitious material. A general discussion of continuity details for prestressed components is also provided. Finally, information compiled from other research projects relevant to the research presented herein is presented.

ULTRA-HIGH PERFORMANCE CONCRETE

UHPC is a term that represents a class of a high-performance, fiber-reinforced, advanced cementitious composites. UHPC has been defined as follows:

> *UHPC is a cementitious composite material composed of an optimized gradation of granular constituents, a water-to-cementitious materials ratio less than 0.25, and a high percentage of discontinuous internal fiber reinforcement. The mechanical properties of UHPC include compressive strength greater than 21.7 ksi (150 MPa) and sustained post-cracking tensile strength greater than 0.72 ksi (5 MPa).[†] UHPC has a discontinuous pore structure that reduces liquid ingress, significantly enhancing durability compared to conventional concrete.*[(1,2)]

The advantages to using UHPC in place of a conventional concrete include enhanced material properties such as noteworthy compressive strength, increased ductility due to steel fiber reinforcement, and superior durability characteristics resulting from its very low permeability.

UHPC has been commercially available for more than a decade in the U.S.; however, the associated knowledge base required for effective design and deployment is just beginning to coalesce. The results compiled in Table 1 present average values for a number of test parameters relevant to the use of UHPC as obtained from independent testing of a commercially available product.[(3)] This research published by the Federal Highway Administration in 2006 investigated a number of material properties of UHPC. The research analyzed both mechanical- and durability-based behaviors of UHPC to validate use in future highway and bridge construction projects.

Table 1. Typical field-cast UHPC material properties.

[†]The tensile behavior of UHPC is generally defined as "strain-hardening," which is a broad term defining concretes wherein the sustained post-cracking strength provided by the fiber reinforcement is greater than the cementitious matrix cracking strength. However, the definitional dependence on cementitious matrix cracking strength may inappropriately include some concretes that exhibit low first-cracking strengths. Note that the post-cracking tensile strength and strain capacity of UHPC is highly dependent on the type, quantity, dispersion, and orientation of the internal fiber reinforcement.

Material Characteristic	Average Result
Density	2,480 kg/m^3 (155 lb/ft^3)
Compressive Strength (ASTM C39; 28-day strength)	126 MPa (18.3 ksi)
Modulus of Elasticity (ASTM C469; 28-day modulus)	42.7 GPa (6200 ksi)
Split Cylinder Cracking Strength (ASTM C496)	9.0 MPa (1.3 ksi)
Prism Flexure Cracking Strength (ASTM C1018; 305-mm (12-in.) span)	9.0 MPa (1.3 ksi)
Mortar Briquette Cracking Strength (AASHTO T132)	6.2 MPa (0.9 ksi)
Direct Tension Cracking Strength (Axial tensile load)	5.5–6.9 MPa (0.8–1.0 ksi)
Prism Flexural Tensile Toughness (ASTM C1018; 305-mm (12-in.) span)	I_{30} = 48
Long-Term Creep Coefficient (ASTM C512; 77 MPa (11.2 ksi) load)	0.78
Long-Term Shrinkage (ASTM C157; initial reading after set)	555 microstrain
Total Shrinkage (Embedded vibrating wire gage)	790 microstrain
Coefficient of Thermal Expansion (AASHTO TP60–00)	14.7 x10^{-6} mm/mm/ºC (8.2 x10^{-6} in./in./ºF)
Chloride Ion Penetrability (ASTM C1202; 28-day test)	360 coulombs
Chloride Ion Permeability (AASHTO T259; 12.7-mm (0.5-in.) depth)	< 0.06 kg/m^3 (< 0.10 lb/yd^3)
Scaling Resistance (ASTM C672)	No Scaling
Abrasion Resistance (ASTM C944 2x weight; ground surface)	0.73 grams lost (0.026 oz. lost)
Freeze-Thaw Resistance (ASTM C666A; 600 cycles)	RDM = 112%
Alkali-Silica Reaction (ASTM C1260; tested for 28 days)	Innocuous

CONTINUITY CONNECTION DETAILS FOR PRESTRESSED COMPONENTS

The size and weight of precast concrete components are frequently limited based on transportation and erection considerations. Precast, prestressed concrete girders can become impractical for medium and long span bridges. For these bridge spans, the use of smaller precast concrete elements combined with post-tensioning technology has proven to be a viable and economical construction technique. For medium span bridges, spliced girders have been shown to be a competitive alternative to traditional bridge systems. NCHRP Report 517 *Extending Span Ranges of Precast Prestressed Concrete Girders* extensively investigated this topic.[(4)]

Common spliced girder bridge construction includes the fabrication of precast, prestressed girder segments, the erection of the girder segments, and the longitudinal post-tensioning of the girder segments to create the bridge superstructure. The splices in these structures tend to include both pretensioned and non-pretensioned reinforcement. Although the post-tensioning installed on these bridges affords the required structural capacity while precompressing the structure and thus enhancing the concrete durability, it also adds complexity and expense to the prefabrication and field construction operations.

Separately, the bridge sector has recently shown an interest in increasing the structural efficiency and durability of simple span precast/prestressed concrete girders by creating a continuous for live load connection over the piers of multispan bridges. In these cases, untensioned prestressing

strand and/or mild steel reinforcement extend from the ends of the abutting girders and are spliced through the use of supplementary reinforcement and a field-cast concrete closure pour.

Parkar et al. recently published a review of continuity connection details for prestressed concrete girders.[5] This study investigated both continuous for live load connection details at support locations (referred to as "on-pier splicing") as well as spliced girder connections at unsupported locations (referred to as "in-span splicing"). This study presented the advantages and disadvantages of a variety of continuity connection concepts. Of particular interest here, it pointed to the simplicity of non-prestressed connections while also mentioning that these connections are more susceptible to cracking than pretensioned connections.

BOND BEHAVIOR OF UNTENSIONED STRAND

The bond behavior of untensioned strand has been investigated in a limited number of relevant studies. Salmons and McCrate investigated the bond strength of untensioned straight, bent, and frayed strands embedded in 3.8 to 6.9 ksi (26 to 47 MPa) conventional concrete.[6] Embedment lengths ranged from 4 to 45 inches (10 to 114 cm), and most tests were completed on 0.5 inch (12.7 mm) diameter strands. The test setup reduced, but did not eliminate, the confining compressive stresses that can increase the bond of embedded reinforcements in concrete.

The focus of the study was on the general bond slip of untensioned strand at lower stress levels, not on the embedment length required to reach the ultimate strand strength. Even so, a few tests on straight, 0.5 inch (12.7 mm) diameter strands were completed wherein the load was increased to as high as 90% of the nominal capacity of the strand. In three of the tests, with embedment lengths of 30, 30, and 45 inches (76, 76, and 114 cm), the strand stress reached this limiting stress level. However, it must be recognized that the test setup did induce confining forces and that reaching the full strand rupture strength may have necessitated significantly longer embedment distances. Based on another part of the study, the authors recommended a design equation that would predict that the full development length of a 0.5 inch (12.7 mm) diameter straight strand would be 99 inches (251 cm).

More recently Chao et al. investigated the bonding of untensioned strands in a variety of fiber reinforced cementitious composites.[7] Straight lengths of 0.5 inch (12.7 mm) diameter, 270 ksi (1860 MPa), 7-wire prestressing strands were cast into 6 by 6 by 4 inch (150 by 150 by 100 mm) prisms. This traditional pullout configuration included reactions on the corners of each prism while the strands were pulled in tension, thus potentially generating confining forces around each strand. These researchers concluded that the inclusion of fiber reinforcement can significantly increase the bond strength and thus shorten the embedment length required for full development of the strand. Particular geometries and volumetric percentages of fibers were found to provide greater enhancement of bond strength.

BOND BEHAVIOR OF TENSIONED STRAND IN UHPC

Bertram and Hegger completed research investigating the bond behavior of strands in a variety of UHPC formulations.[8] This work was completed as part of the priority program on UHPC

development funded by the German Research Foundation (DFG) at universities around Germany. The study investigated the impact of the Hoyer effect, the strand cover, the strand size, and the UHPC steel fiber concentration on the bond stress of the strand in the UHPC. The volumetric fiber reinforcement ratios tested ranged from 0.9 to 2.5 percent.

The pullout testing portion of the study focused on very short embedment lengths in order to determine the bond stress between the strand and the UHPC. The results of this part of the study indicated that the bond stress varies from approximately 1.9 ksi (13 MPa) when the Hoyer effect is not present to approximately 4.3 ksi (30 MPa) when a significant Hoyer effect is present. The no-Hoyer effect situation is similar to that encountered during the pullout of an untensioned strand. These results pertain to specimens with sufficient cover or other confinement to eliminate the possibility of a splitting failure wherein the bond resistance is greatly reduced. Given the bond stresses are necessarily greater near the loaded end of the embedded strand, a progressive splitting failure must be considered when extending the Bertram and Hegger results to longer embedment lengths.

These pullout tests also indicated that a concrete cover at least 2.5 times thicker than the diameter of the prestressing strand would significantly reduce the likelihood of a splitting failure. For a 0.5 inch (12.7 mm) strand, this cover distance equates to 1.25 inches (32 mm).

A separate phase of this study investigated the transfer length of prestressing strands in small, prestressed I-beams. The authors report that the transfer length ranged from 8.7 to 11 inches (22 to 28 cm). This result is instructive as it provides an indication of the lower bound for the development length.

CHAPTER 3. TEST MATRIX, MATERIALS, AND SPECIMENS

INTRODUCTION

The test matrix and test specimen details are presented first in this chapter. Thereafter, details regarding the batching, mixing, and casting of the UHPC test specimens are presented. Finally, the compression mechanical responses of the four UHPC batches are presented.

TEST MATRIX

The objective of this research project was to determine the non-contact lap splice length of prestressing strands embedded in UHPC. The primary variables investigated included the type of fiber reinforcement in the UHPC, the diameter of the prestressing strand, and the length of the lap splice. The 270-ksi (1860-MPa) low relaxation prestressing strands were either 0.5 inch (12.7 mm) diameter or 0.6 inch (15.2 mm) diameter. The UHPC fiber reinforcement was straight cylindrical fibers composed of either steel or polyvinyl alcohol (PVA) that were included in the mix design at a volumetric ratio of two percent. The lap splice lengths varied from as short as 8 inches (203 mm) to as long as 36 inches (914 mm).

The test matrix is provided in Table 2. This table delineates the four specimen groups and provides the variables addressed by each of the 18 specimens. The design of the specimens is discussed in the next section.

TEST SPECIMEN DETAILS

The test specimens all used a similar overall geometry, with the primary variable being the length of the lap splice. Figure 1 provides the geometry of the test specimen along with the loading configuration setup. All specimens had an overall cross section of 3 by 5 inches (76 by 127 mm). The middle strand was centered in this cross section, while the two outside strands were centered 1 inch (25.4 mm) on either side along the 5 inch (127 mm) length. This configuration simulated the interlacing of prestressing strands that might extend from a precast element cast with strands on 2 inch (51 mm) centers.

Since the overall cross-sectional dimensions remained constant throughout the series of test specimens, the cover on the strands necessarily varied depending on the size of the strand. For 0.5 inch (12.7 mm) diameter strands, the cover to the shorter and longer free edges was 1.25 inches (32 mm). This cover corresponds to the minimum cover recommended for 0.5 inch (12.7 mm) diameter strands by Bertram and Hegger.[8] For the 0.6 inch (15.2 mm) diameter strands, the cover to the shorter and longer free edges was 1.20 inches (30.5 mm).

Each end of each strand extended beyond the end faces of the test specimen. The longer strand tails served as the loading attachments onto which strand chucks were inserted. The shorter single tail served as an attachment point onto which was mounted the linear variable differential transformer (LVDT) that measured strand slip.

The prestressing strands used in this study were standard low relaxation 270 ksi (1860 MPa) strands obtained from a precast concrete component manufacturer. The strands were sealed in bundles and stored indoors between acquisition from the precast concrete component manufacturer and casting into the test specimens.

Table 2. Test Matrix

Specimen Group	Specimen Name	UHPC Fiber Type	Prestressing Strand Size, in. (mm)	Lap Splice Length, in. (mm)
R2A	R2A01	Steel	0.5 (12.7)	8 (203)
	R2A02			12 (305)
	R2A03			16 (406)
	R2A04			20 (508)
	R2A05			24 (610)
R2B	R2B01	PVA	0.5 (12.7)	8 (203)
	R2B02			12 (305)
	R2B03			16 (406)
	R2B04			20 (508)
	R2B05			24 (610)
R2C	R2C01	PVA	0.5 (12.7)	24 (610)
	R2C02			30 (762)
	R2C03			36 (914)
R2D	R2D01	Steel	0.6 (15.2)	8 (203)
	R2D02			12 (305)
	R2D03			16 (406)
	R2D04			20 (508)
	R2D05			24 (610)

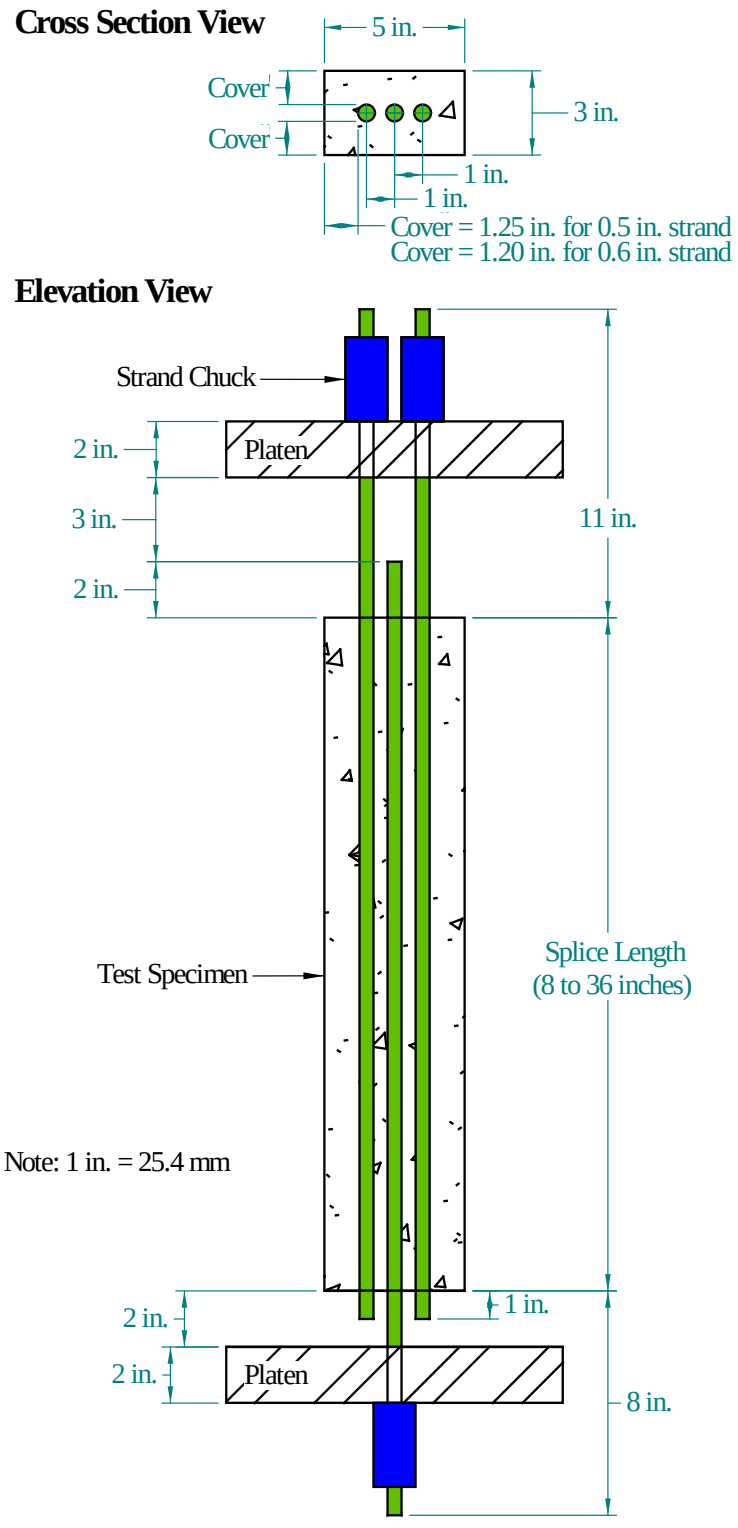

Figure 1. Illustration. Test specimen geometry and loading setup.

UHPC MIX DESIGN, MIXING, AND CASTING

The UHPC used for this research was obtained from the manufacturer, Lafarge North America. The specific products tested were Ductal JS1100-RS and Ductal JS2100-RS, each of which is a rapid-setting formulation of this manufacturer's traditional UHPC product. The only difference between these two products is that the first includes steel fiber reinforcement while the second includes polyvinyl alcohol (PVA) fiber reinforcement. This concrete is similar to other products in the same UHPC product line in that the constituents include a blended cementitious premix powder, water, water-reducing admixtures, and steel fiber reinforcement. The premix includes a blend of silica fume, ground quartz, sand, and cement. Though the proportions of each are proprietary for this UHPC, approximate quantities of constituents in this product line have been documented in other research studies.[(3)] These proportions for a steel fiber reinforced mix design are provided in Table 3.

Table 3. Typical UHPC mix composition.

Material	Amount (lb/yd^3 (kg/m^3))	Percent by Weight
Portland Cement	1,200 (712)	28.5
Fine Sand	1,720 (1,020)	40.8
Silica Fume	390 (231)	9.3
Ground Quartz	355 (211)	8.4
Superplasticizer	51 (30)	1.2
Steel Fibers	263 (156)	6.2
Water	218 (130)	5.2

The mix designs used in this study represent the standard mix designs for this family of UHPC products from this manufacturer. The mix designs are discussed below and presented in Table 4 and Table 5. The two water-reducing admixtures in the mix designs are products of Chryso, Inc. and were recommended by the UHPC supplier. Fluid Optima 100 is a modified phosphonate plasticizer. Fluid Premia 150 is a modified polycarboxylate high-range water-reducing admixture. Optima 100 and Premia 150 were included in batches according to the UHPC-supplier's recommended mix proportions.

The steel fibers included in this mix design were nondeformed, cylindrical, high-tensile strength steel. They have a diameter of 0.008 in. (0.2 mm) with a length of 0.5 in. (12.7 mm). The steel fibers have a thin brass coating which provides lubrication during the drawing process and provides corrosion resistance for the raw fibers. Steel fibers in this manufacturer's UHPC products are generally proportioned as a percent of total volume, commonly at two percent. Table 4 provides the mix proportions based on a 1-ft^3 (0.028-m^3) design yield.

The PVA fibers supplied with the UHPC were nondeformed, cylindrical fibers with a tensile strength of 145 ksi (1 GPa) and a modulus of elasticity of 4200 ksi (29 GPa). Manufactured by Kuralon and marketed as fiber RF350, they have a diameter of 0.008 in. (0.2 mm), a length of

0.47 in. (12 mm), and a density of 81 lb/ft^3 (1.3 g/cm^3). These fibers were included in the mix at two percent of the total mix volume. Table 5 provides the mix proportions based on a 1-ft^3 (0.028-m^3) design yield. Note that this mix design includes a higher water content in order to facilitate mixing and placing of the material.

Table 4. Mix Proportions for UHPC with Steel Fibers

Material	Amount (lb/ft^3 (kg/m^3))	Percent by Weight
Premix	137.029 (2195)	86.7
Water	9.364 (150)	5.9
Premia 150	1.124 (18)	0.7
Optima 100	0.749 (12)	0.5
Steel Fibers	9.739 (156)	6.2

Table 5. Mix Proportions for UHPC with PVA Fibers

Material	Amount (lb/ft^3 (kg/m^3))	Percent by Weight
Premix	137.029 (2195)	90.88
Water	10.301 (165)	6.83
Premia 150	1.124 (18)	0.75
Optima 100	0.749 (12)	0.50
PVA Fibers	1.573 (25.2)	1.04

Mixing of the UHPC was achieved through the use of a 1930s era pan mixer with a capacity of 2 ft^3 (0.057 m^3). Mixing times varied depending on the age of the premix since blending, but were generally between 12 and 18 minutes. The design yield of each of the four batches was 1 ft^3 (0.028 m^3).

The mixing process used for the UHPC-RS differed from that used for conventional concrete due to the nature of the material. As per the UHPC supplier's recommendation, both the Premia and Optima were added directly to the mixing water. The premix powder was added to a dry mixing pan and mixing began. Over the course of the first two minutes, the liquids were added slowly and consistently to the premix. When the material could be considered a flowable paste, the fibers were added over the course of one minute. Once the fibers appeared to be sufficiently incorporated, which required approximately three minutes, mixing ceased and the molds were filled.

The test specimens were cast into open top molds with wood sides and steel base plates. The end plates through which the strands passed were polycarbonate. Figure 2 provides a photo of a 12 inch (305 mm) long test specimen with 0.5 inch (12.7 mm) diameter strands immediately prior to the casting of the UHPC.

The casting of the UHPC was completed from one batch of UHPC for each set of specimens. The flowable UHPC was poured into the mold using a scoop. The scoop was positioned to deposit the UHPC in the center of the mold, allowing the UHPC to flow toward both ends. The

fluidity of the UHPC allowed it to completely fill each of the molds without difficulty. Figure 3 shows the casting of a 20 inch (508 mm) long test specimen. Immediately after filling the mold, each mold was briefly vibrated on a vibrating table to speed the release of air entrapped during the casting process. Then the open surface of each specimen was screeded and finished with a magnesium hand float to ensure that the mold was not overfilled. Finally, a plastic sheet was pressed onto the exposed UHPC surface.

The test specimens remained in the standard laboratory environment in which they were cast for one day. At that time the specimens were stripped then placed in a room with constant 73°F (23°C) temperature and 50% relative humidity. The specimens remained in this room until testing.

Figure 2. Photo. Form with strands for 12 inch (30.5 cm) long test specimen.

Figure 3. Photo. Casting of a 20 inch (50.8 cm) long test specimen.

COMPANION COMPRESSION MECHANICAL TESTING

Alongside each batch of pullout test specimens, a set of six compression test cylinders were cast. All cylinders were 3 in. (76.2 mm) nominal diameter with approximately 6 in. (152.4 mm) lengths. These cylinders were cast immediately after the pullout test specimens in each batch. After each cylinder mold was filled, the cylinder was briefly vibrated on a vibrating table to assist in the release of entrapped air. The cylinders were then finished with a magnesium hand float and covered in plastic. The cylinders were cured alongside the pullout test specimens.

The compressive mechanical testing was completed through modified versions of the ASTM C39 *Standard Test Method for Compressive Strength of Cylindrical Concrete Specimens* and ASTM C469 *Standard Test Method for Static Modulus of Elasticity and Poisson's Ratio of Concrete in Compression* tests.[9,10] The employed test method has been engaged multiple times in the past to capture the stress-strain response of UHPC.[3,11,12] In these tests, the axial load and axial strain on the cylinder were collected from initial load application through failure of the specimen. As such, the compressive stress-strain responses through the attainment of the compressive strength were captured.

From the standpoint of the ASTM C39 test method, the two modifications included that the load rate was increased and that the axial strain was captured during the test. The specified loading rate of 35 psi/second (0.24 MPa/second) was changed to 150 psi/second (1.0 MPa/second) due to the high compressive strength of UHPC and the duration of test that would result from the slower load rate.

The axial strain was measured through the use of a parallel ring compressometer. This device is similar to the traditional compressometer described in ASTM C469, except that it holds three LVDTs and does not use a hinge to proportionally increase the observed deformations. The top ring held the three LVDTs spaced equidistant around the perimeter of the ring and which bore down onto the bottom ring. The gage length between the centers of the two rings was set at 2 in. (50.8 mm). Using this apparatus, the axial deformation of the cylinder was measured and recorded throughout the entire compressive loading of the cylinder.

Data acquisition of the loads and displacements was accomplished with a laptop computer and software designed to connect and communicate with both the compression test machine and the three LVDTs. The main body of ASTM C469 specifies the test be completed in a minimum of two separate loadings, with the first set of load data being discarded. Loading should not exceed 40 percent of the peak compressive strength (ultimate load). Testing for this study, however, followed the alternative given in Section 6.5 of ASTM C469, which allows for the simultaneous collection of both compressive strength and modulus of elasticity, so long as the displacement measurement device(s) is/are either protected from damage at failure or disposable.

The three specific parameters captured during each test included the compressive strength, the modulus of elasticity, and the strain at peak strength. Stresses are defined as the applied load divided by the average cross-sectional area. Strains are defined as the average axial deformation divided by the gage length. The compressive strength and the strain at peak strength were both captured at the peak load applied to each cylinder. The modulus of elasticity was calculated based on a linear best-fit approximation of the slope of the stress-strain response between 10

percent and 30 percent of the peak stress applied to a specimen. Given that the stress and strain data were collected through the entire test, post-processing of the data allowed the modulus of elasticity to be calculated over this precise stress range for each specimen.

Prior to testing, both ends of each specimen were ground plane through the use of a cylinder end grinder. After grinding, the ends were verified to be within 0.5 degrees of parallel. Subsequently, each cylinder was measured for diameter, length, and weight. The tests on all six cylinders in each set were completed on the same day. The four sets of cylinders were each tested between 28 and 32 days after casting.

All cylinders were tested in a Forney compression testing machine having a 1,000-kip (4.45-kN) capacity. This hydraulic actuated testing machine uses a needle value to set an oil flow rate. As such, the flow rate was set early in each test so that the appropriate load rate was achieved during the stiffest portion of the response. The oil flow rate was not modified as each specimen neared failure.

The test results for all of the tested cylinders are presented in Table 6. The density, the compressive strength (f_c'), the elastic modulus (E_c), and the strain at peak stress are provided in the table for each specimen. Average results are also presented.

The density, compressive strength, and modulus of elasticity of the steel fiber reinforced batches (R2A and R2D) were observed to be approximately 155 lb/ft^3 (2480 kg/m^3), 23.5 ksi (162 MPa), and 7400 ksi (51 GPa), respectively. For the PVA fiber reinforced batches, these values were approximately 145 lb/ft^3 (2320 kg/m^3), 19 ksi (131 MPa), and 6800 ksi (47 GPa). These results demonstrate that the PVA fiber reinforced batches exhibited lesser compressive mechanical responses. These reduced responses likely are attributable to a combination of the comparatively higher water contents in these batches and to the lower strength/lower stiffness of the PVA fiber reinforcement.

Table 6. Compression testing results.

Batch	Cylinder Number	Density [lb/ft^3]	f_c'		E_c		Strain at f_c'	
			[ksi]	Avg [ksi]	[ksi]	Avg [ksi]		Avg
R2A	1	154.8	24.21	23.3	7820	7600	0.003441	0.003370
	2	154.3	22.82		7360		*	
	3	155.7	24.08		7550		0.003577	
	4	154.3	23.22		7740		0.003112	
	5	154.8	23.04		7430		0.003352	
	6	156.1	22.43		7720		*	
R2B	1	146.5	21.90	20.9	6950	6860	0.003488	0.003490
	2	146.9	22.19		7140		0.003344	
	3	146.1	20.76		6610		0.003645	
	4	146.8	18.39		6790		*	
	5	146.3	20.20		6820		0.003334	
	6	146.4	22.19		6860		0.003647	
R2C	1	145.8	20.42	18.4	7100	6730	0.003228	0.003050
	2	145.6	18.62		6520		0.003144	
	3	145.0	17.10		7350		0.002784	
	4	144.5	18.55		6570		0.003141	
	5	144.6	18.04		6540		0.003068	
	6	143.3	17.62		6290		0.002943	
R2D	1	152.8	23.54	23.6	7300	7280	0.003722	0.003840
	2	152.2	23.15		7310		*	
	3	153.1	23.81		7420		0.003692	
	4	151.5	22.64		7230		*	
	5	153.3	24.40		7160		0.004101	
	6	153.4	23.97		*		*	

Note: 1 ksi = 6.895 MPa, 1 lb/ft^3 = 16.02 kg/m^3

* Strain data not captured correctly throughout the appropriate load range, thus result not reported.

CHAPTER 4. PULLOUT TEST RESULTS

INTRODUCTION

The test results from the physical testing of the strand pullout test specimens are presented in this chapter. First, the test procedure is presented. Next the test results are presented, including data and observations captured during the testing. Finally, the results are analyzed and compared to prior test results and prediction equations.

TEST PROCEDURE

A 100-kip (445-kN) capacity uniaxial testing frame with a computer controlled, closed-loop hydraulic actuator was used for all of the pullout tests. The tests were completed under constant displacement control at an actuator displacement rate of 0.04 inches/minute (1 mm/minute). The load, actuator displacement, and strand slip were measured continuously throughout the test. The strand slip was measured by a 0.5-inch (12.7-mm) range LVDT mounted on the unloaded end of the single strand. These three data points were electronically recorded at 2 Hz.

The test setup is shown in Figure 4. The upper loading fixture is attached to the load cell. The lower loading fixture is attached to the hydraulic actuator. The pair of strands is pulled by the upper load fixture through a rocker bearing. This bearing allows the two strands to pass through and be secured to the chucks while simultaneously accounting for any non-equal seating of the chucks on the strands. The LVDT is attached to the middle strand near the upper load fixture. The lower load fixture includes a slotted hole to allow for easier insertion and removal of test specimens.

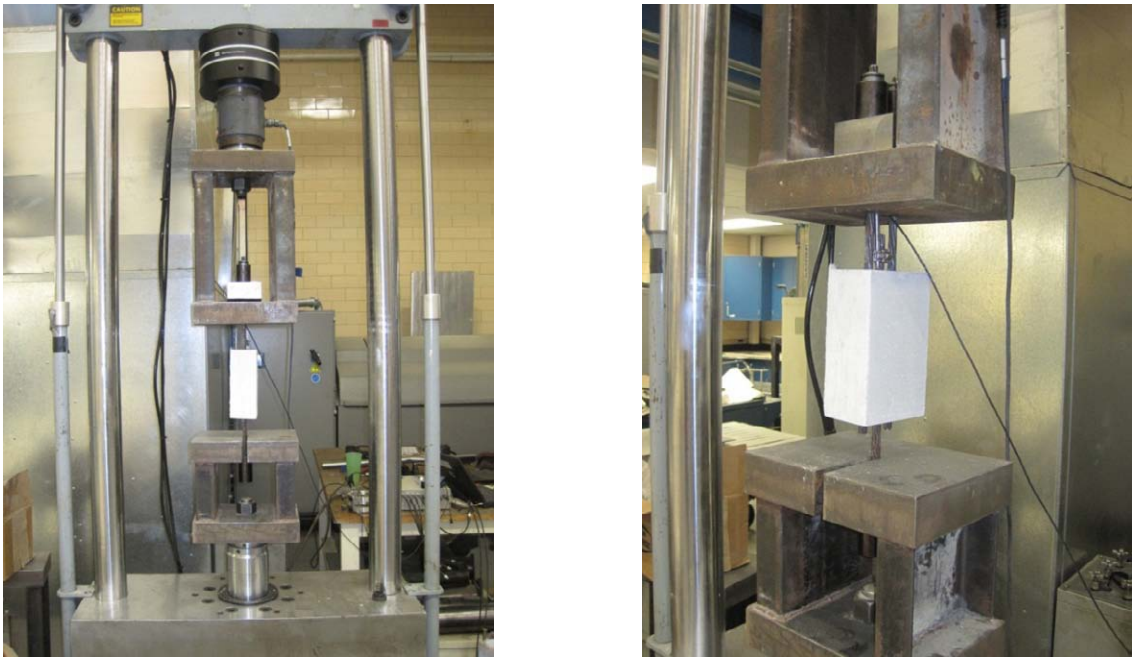

(a) (b)

Figure 4. Photo. (a) Overall and (b) close-up view of test specimen in load frame.

Each of the four sets of specimens was tested between 28 and 32 days after casting. The tests on each series of test specimens were completed sequentially over the course of approximately four hours. After each test, each specimen was saved for further documentation of damage.

TEST RESULTS

The results from the four sets of test specimens are combined into three data sets and presented in this section. The R2B and R2C sets of specimens are combined since, together, they offer a single data set covering a wide range of splice lengths for a specific strand size and fiber type.

R2A – 0.5-Inch (12.7-mm) Diameter Strand with Steel Fiber Reinforcement

The five test specimens in this group exhibited a range of behaviors. The electronically captured load versus actuator displacement results are presented in Figure 5, and the load versus strand slip LVDT results are presented in Figure 6. The photos of the specimens after the completion of the tests are provided Figure 7. The dimensionally largest formed surface is shown for R2A01, R2A02, and R2A03, while the opposing face is shown for R2A04 and R2A05. The open face is shown for the last two since the cracking was most apparent on this face.

All five specimens exhibited similar load-displacement responses up to an applied load of approximately 23 kips (100 kN). At this point, R2A01 with an 8-inch (203-mm) lap splice length began to exhibit significantly increased strand movement and actuator displacement. Although not specifically documented during the test, it is likely that this change in behavior represents the point where a full length split appeared in the test specimen, allowing the center strand to more easily slide through the specimen. The test was stopped when the stroke on the LVDT was exhausted. At the conclusion of the test, a full-length split was observed to run the length of both sides of the test specimen. The only other cracks observed were radial and circumferential cracks near the entry point of the single strand on the loaded end of the specimen.

R2A02 with a 12-inch (305-mm) lap splice length began to exhibit small strand slippage at a slightly higher load, but continued carrying an increasing load until a full-length split was observed to occur at approximately 32 kips (142 kN) of applied load. The full-length split coincided with a loud cracking sound. It is likely that minor cracking of the specimen may have initiated near the loaded end of the center strand prior to the full-length split, thus allowing for the early strand movement. After the splitting of the specimen, the load decreased then rebounded to a nearly steady state wherein the strand slid through the UHPC. The test was stopped then the stroke on the LVDT was exhausted. The full-length splitting crack only occurred on the side of the specimen shown in Figure 7. The only other cracks observed were radial and circumferential cracks near the entry point of the single strand on the loaded end of each specimen.

R2A03 with a 16-inch (406-mm) lap splice length exhibited very little strand movement until approximately 31 kips (138 kN) of applied load. Thereafter, the specimen began to show increasing strand movement as the load increased, with the two notable small load decreases, until the full-length split was observed to occur at an applied load of 40.5 kips (180 kN). Again, the full-length splitting crack coincided with a loud cracking sound. It is likely that minor cracking of the specimen may have initiated near the loaded end of the center strand prior to the

full-length split, thus allowing for the early strand movement. After the splitting of the specimen, the load decreased then rebounded until the test was stopped. The full-length splitting crack only occurred on the side of the specimen shown in Figure 7. The only other cracks observed were radial and circumferential cracks near the entry point of the single strand on the loaded end of each specimen. This test specimen reached 98% of the nominal strand strength. It is likely that some of the deformation observed in Figure 5 relates to yielding of the prestressing strand as the peak load was approached.

Test specimens R2A04 with the 20-inch (508 mm) length and R2A05 with the 24-inch (610-mm) length both displayed similar behaviors. In each case, the specimen showed minimal strand movement prior to the strand rupturing at its ultimate capacity. The rupture loads were 41.6 kips (185 kN) and 42.2 kips (188 kN) for R2A04 and R2A05, respectively. Neither of these specimens exhibited any splitting cracks. Instead, they each exhibited tensile cracks consistent with the generation of tensile forces in the UHPC parallel to the line of action of the applied forces on the strands. The open cast faces of these two specimens are shown, with each one exhibiting approximately four continuous cracks across the face. These specimens also exhibited radial and circumferential cracks near the entry point of the single strand on the loaded end of each specimen. It is likely that some of the deformation observed in Figure 5 relates to yielding of the prestressing strand as the peak load was approached.

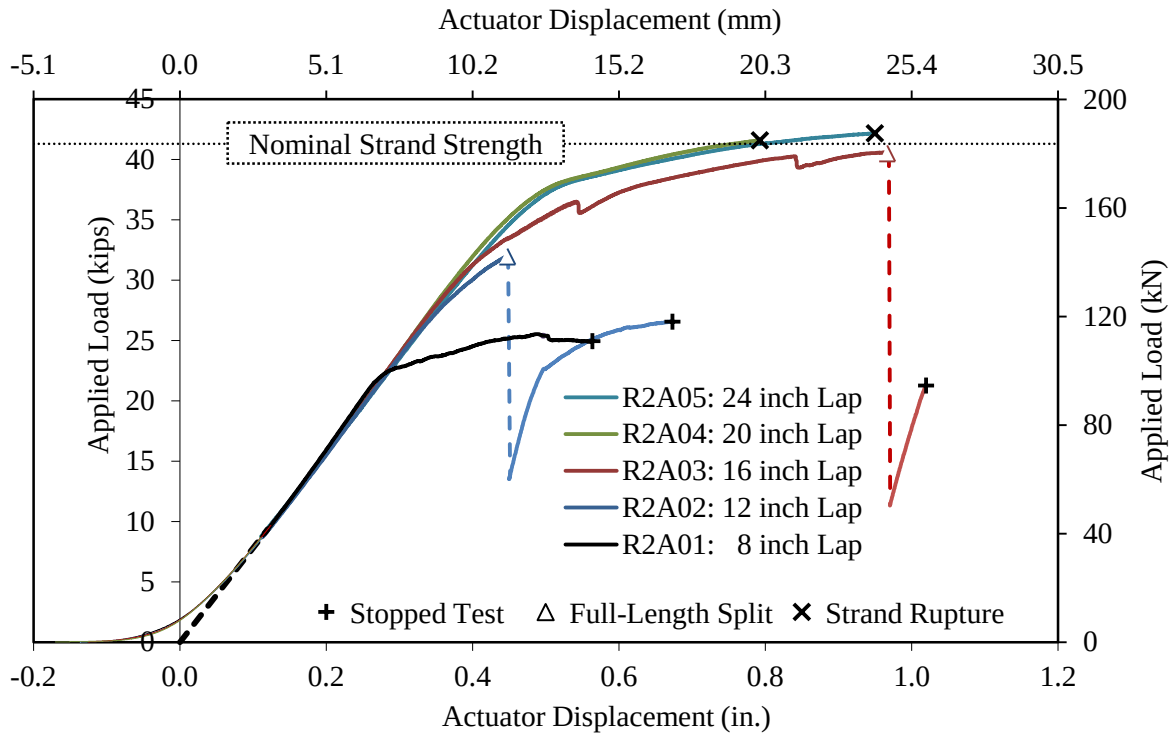

Figure 5. Graph. Load versus actuator displacement response for R2A specimens.

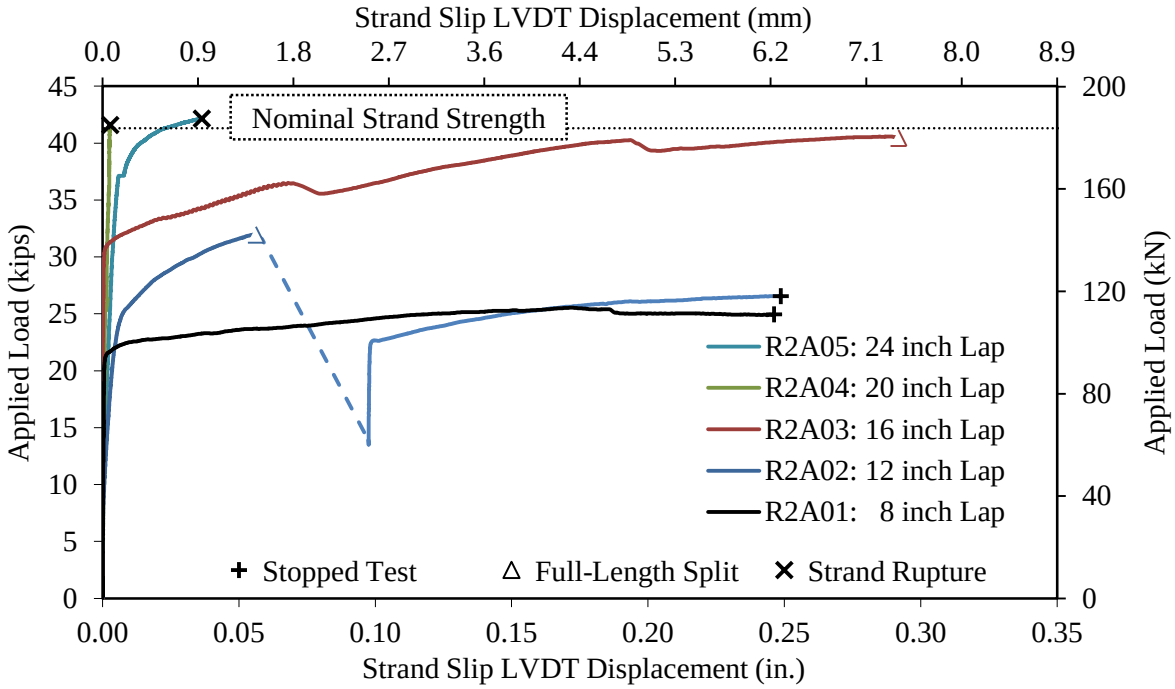

Figure 6. Graph. Load versus strand slip response for R2A specimens.

R2A01

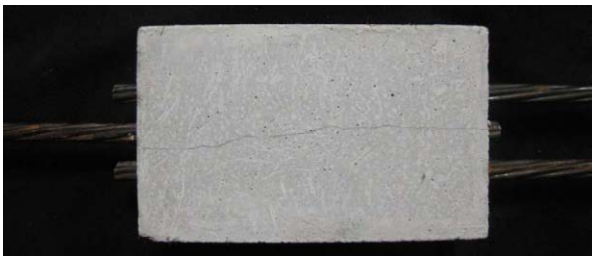

R2A02

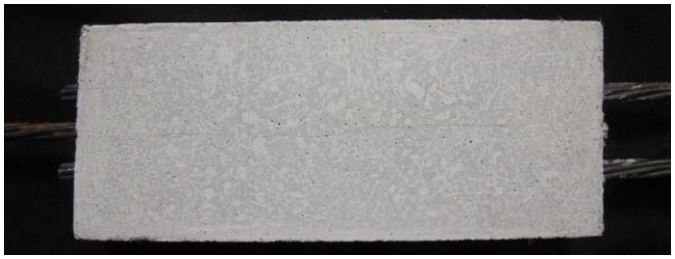

R2A03

R2A04

R2A05

Figure 7. Photographs. Cracking apparent at conclusion of testing of R2A specimens.

R2B and R2C – 0.5-Inch (12.7-mm) Diameter Strand with PVA Fiber Reinforcement

The eight test specimens in this group exhibited a range of behaviors. The electronically captured load versus actuator displacement results are presented in Figure 8, and the load versus strand slip LVDT results are presented in Figure 9. The photos of the specimens after the completion of the tests are provided Figure 10 for the R2B specimens and Figure 11 for the R2C specimens. The dimensionally largest formed surface is shown for all eight test specimens as this face clearly shows the most significant cracking that was apparent at the conclusion of the tests.

The first seven test specimens all exhibited similar behavior. In each case, the load and actuator displacement increased uniformly until the peak load was reached. Peak load coincided with the appearance of a full-length splitting crack. The occurrence of this crack allowed for a reduction in the confining force on the center strand, thus reducing the friction force and allowing for movement of the strand at a reduced applied load level. It must be noted that the stiffness of some of the longer lap spliced specimens was observed to decrease as transverse cracks and partial length splitting cracks appeared, along with the likely initiation of strand yielding, prior to the attainment of peak load.

The longest lap spliced specimen, R2C03, exhibited different behavior. This test specimen exhibited very little strand slip while the specimen as a whole exhibited a significant amount of ductility as the peak load was approached. The load peaked at 42.7 kips (190.0 kN), which is 3.4% higher than the 41.3 kip (183.7 kN) nominal strand strength. As the peak load was approached, additional transverse cracks and partial length splitting cracks appeared, and the strand likely began to yield. The extent of inelastic behaviors was eventually sufficient to allow the strand to more freely slip and for the load to decrease. No full length splitting crack occurred.

In all cases, the post-peak strand slip behavior of the test specimens was similar. In a general sense, the load can be described as initially decreasing but then stabilized at a nearly constant level while the strand pulls through the test specimen. This load level can be viewed as the resistance to sliding friction within each test specimen.

The cracking apparent in each of the five R2B specimens at the conclusion of testing is shown in the photographs in Figure 10. All of the specimens exhibited a full length split from the center strand to the surface shown. R2B01, R2B02, and R2B04 exhibited full length splits on both the formed and open cast sides of the specimens closest to the center strand. R2B03 and R2B05 exhibited full length splits on the formed side and partial length splits on the open cast side. R2B02 through R2B05 also exhibited transverse cracks indicative of the generation of longitudinal tensile forces in the UHPC. The intersections of the longitudinal (i.e., splitting) and transverse cracks indicates that some of the transverse cracks appeared prior to the appearance of the intersecting splitting crack. Specimens R2B02, R2B03, R2B04, and R2B05 displayed 1, 2, 5, and 5 transverse cracks, respectively. Each of the specimens also displayed radial and circumferential cracks near the entry point of the single strand on the loaded end of the specimen.

The cracking apparent in each of the three R2C specimens at the conclusion of testing is shown in the photographs in Figure 11. R2C01 and R2C02 exhibited a full length split from the center

strand to the surface shown, while R2C03 exhibited a partial length split. Each of these three specimens also exhibited a partial length split on the open cast sides of the specimens closest to the center strand. All three specimens also exhibited transverse cracks indicative of the generation of longitudinal tensile forces in the UHPC. The intersections of the longitudinal (i.e., splitting) and transverse cracks indicates that some of the transverse cracks appeared prior to the appearance of the intersecting splitting crack. Specimens R2C01, R2C02, and R2C03 displayed 3, 9, and 12 transverse cracks, respectively. Each of the specimens also displayed radial and circumferential cracks near the entry point of the single strand on the loaded end of the specimen.

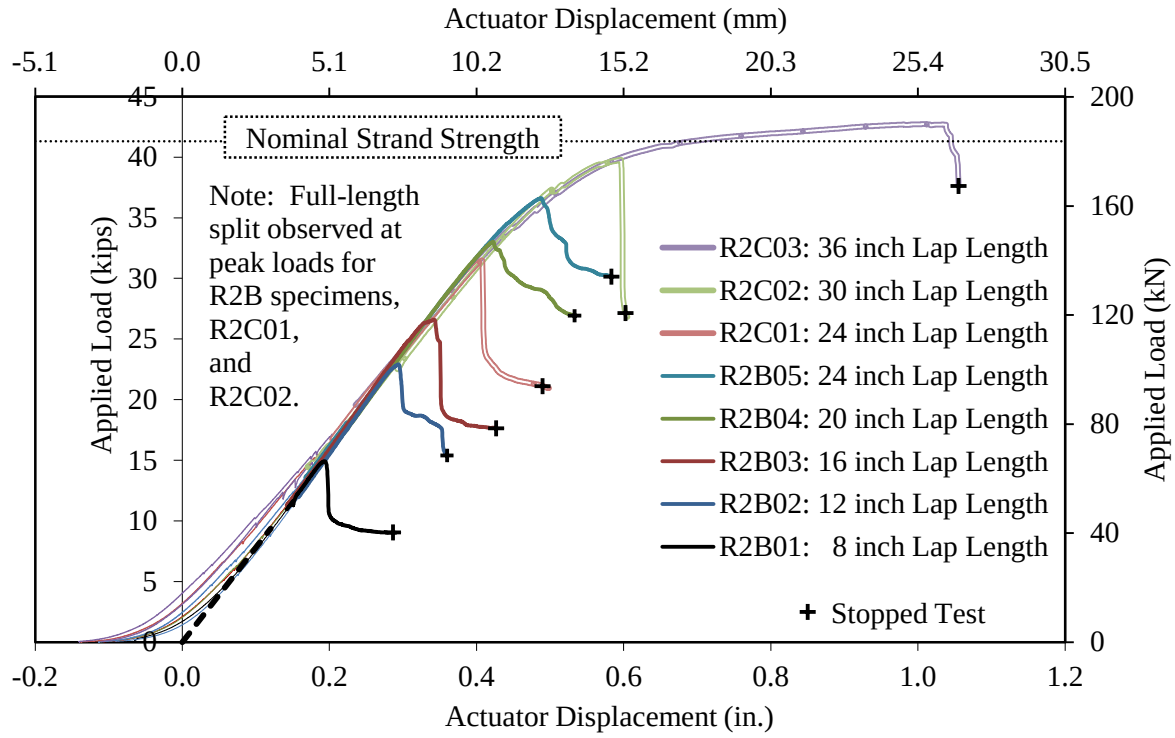

Figure 8. Graph. Load versus actuator displacement response for R2B and R2C combined specimen set.

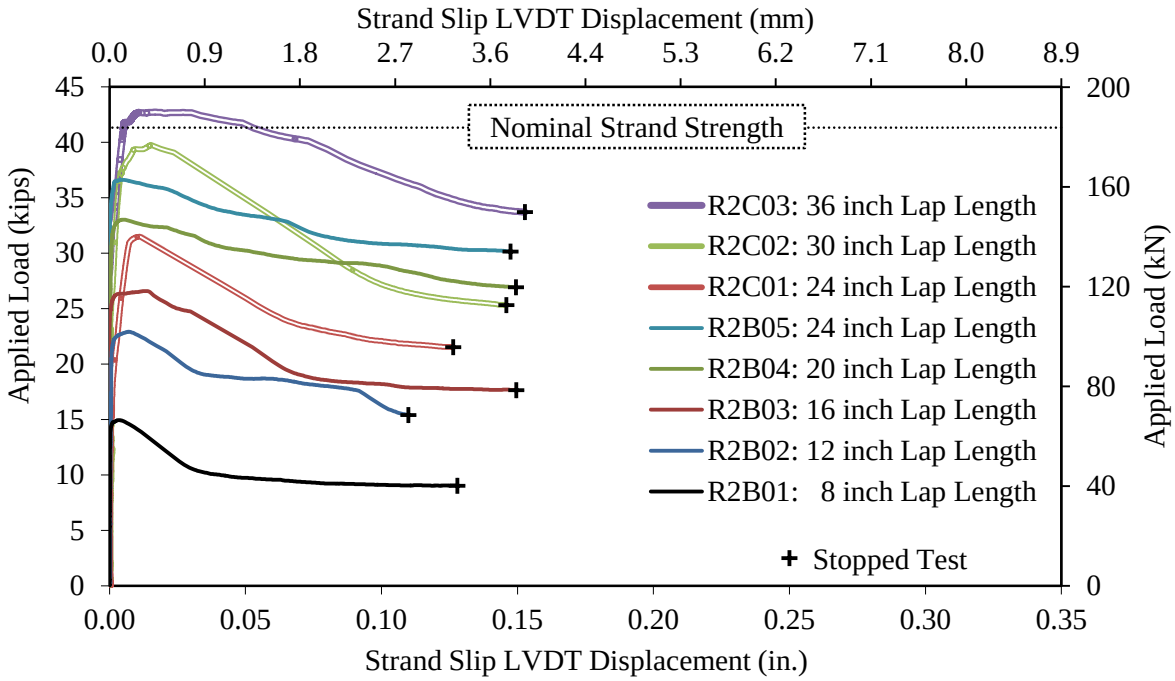

Figure 9. Graph. Load versus strand slip response for R2B and R2C combined specimen set.

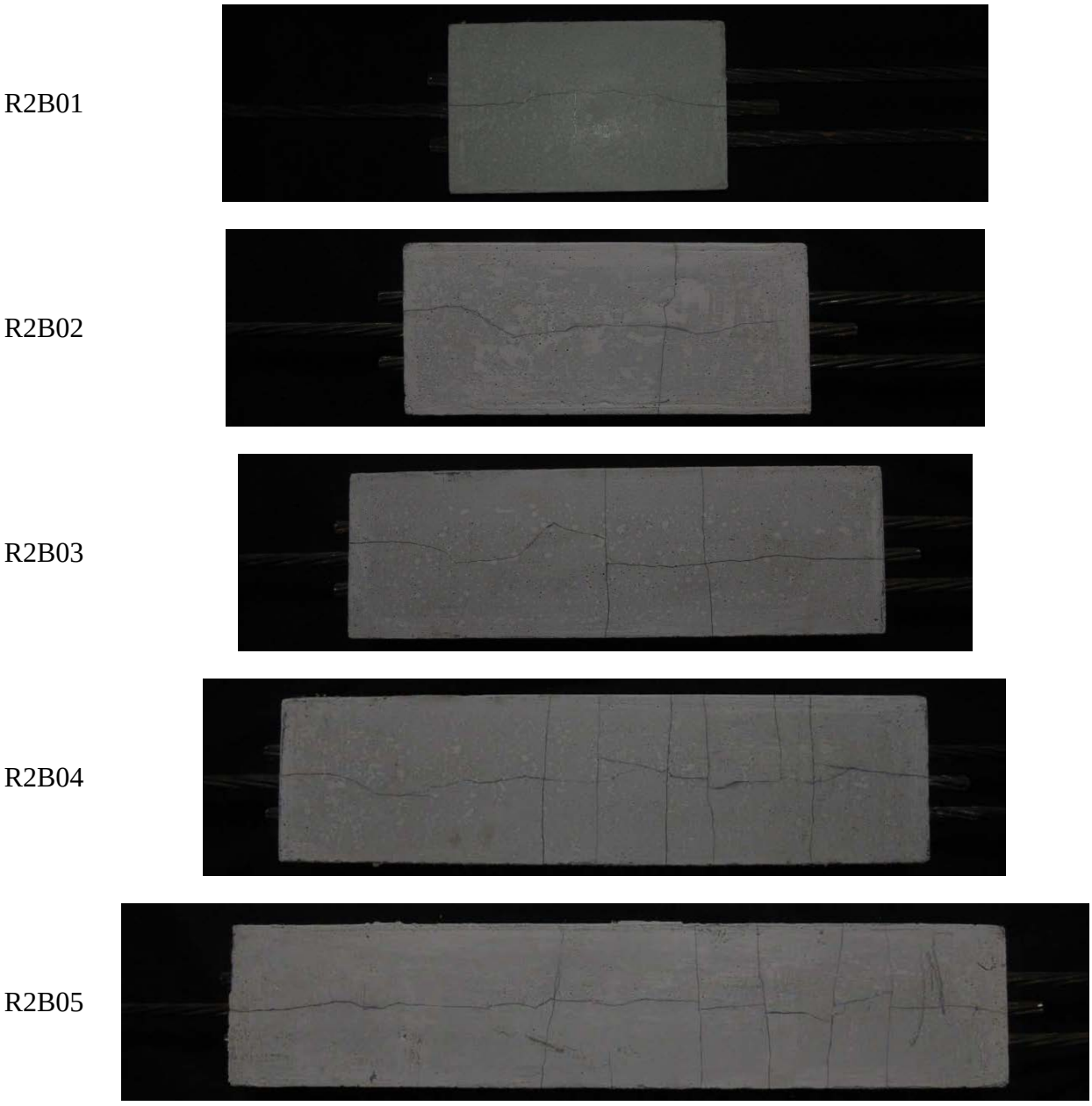

Figure 10. Photographs. Cracking apparent at conclusion of testing of R2B specimens.

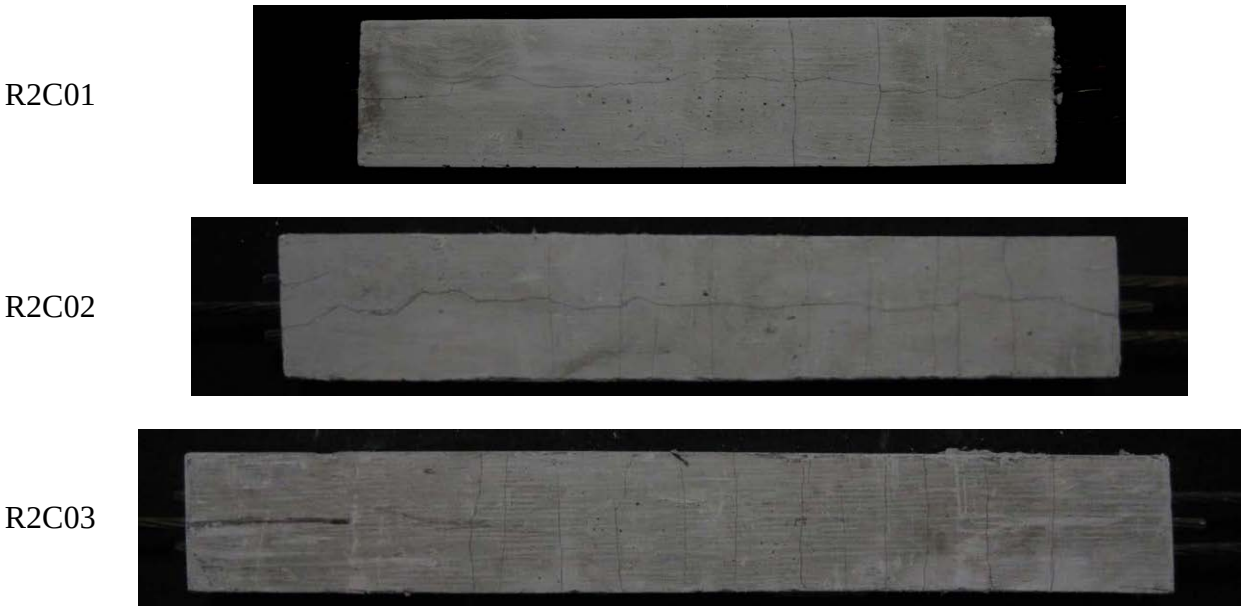

Figure 11. Photographs. Cracking apparent at conclusion of testing of R2C specimens.

R2D – 0.6-Inch (12.7-mm) Diameter Strand with Steel Fiber Reinforcement

The electronically captured load versus actuator displacement results for the five test specimens in this set are presented in Figure 12. The load versus strand slip LVDT results are presented in Figure 13. The photos of the specimens after the completion of the tests are provided Figure 14. The dimensionally largest formed surface is shown for all five test specimens.

All five specimens exhibited similar load-displacement responses up to an applied load of approximately 23 kips (100 kN). At this point, R2D01 with an 8-inch (203-mm) lap splice length began to exhibit significantly increased strand movement and actuator displacement. This change in behavior coincides with the appearance of the full-length splitting crack, which allowed the center strand to more easily slide through the specimen.

Specimens R2D02, R2D03, and R2D04 exhibited similar overall behaviors, with the splitting crack and load decrease occurring at 33 kips (147 kN), 38 kips (169 kN), and 50.2 kips (223 kN), respectively.

Specimens R2D01 through R2D04 all exhibited a full length split from the center strand to the surface shown in Figure 14. These specimens also exhibited a partial length split on the opposing face beginning at the end with the loaded single strand and terminating within 4 inches (10 cm). None of the specimens exhibited transverse cracking. All of the specimens displayed radial and circumferential cracks near the entry point of the single strand on the loaded end of the specimen.

The longest lap spliced specimen, R2D05, exhibited somewhat different behavior. After this specimen exceeded the load level sustained by the shorter specimens, this test specimen exhibited very little strand slip while simultaneously exhibiting a significant amount of overall ductility as the peak load was approached. This ductility corresponds to overall extension of the test specimen primarily attributable to the straining/yielding of the strand, but not to the slipping of the dead end of the strand. The load peaked at 60.7 kips (270 kN), which is 3.6% higher than the 58.6 kip (260.7 kN) nominal strand strength. As the peak load was approached, partial length splitting cracks appeared. As with the other specimens in this set, at peak load the splitting crack reached full length and the load decreased. At the conclusion of the test, the specimen displayed radial and circumferential cracks near the entry point of the single strand on the loaded end of the specimen.

In all five test specimens, the post-peak strand slip behavior of the test specimens was similar. In a general sense, the load can be described as initially decreasing but then stabilizing at a nearly constant level while the strand pulled through the test specimen. This load level can be viewed as the resistance to sliding friction within each test specimen.

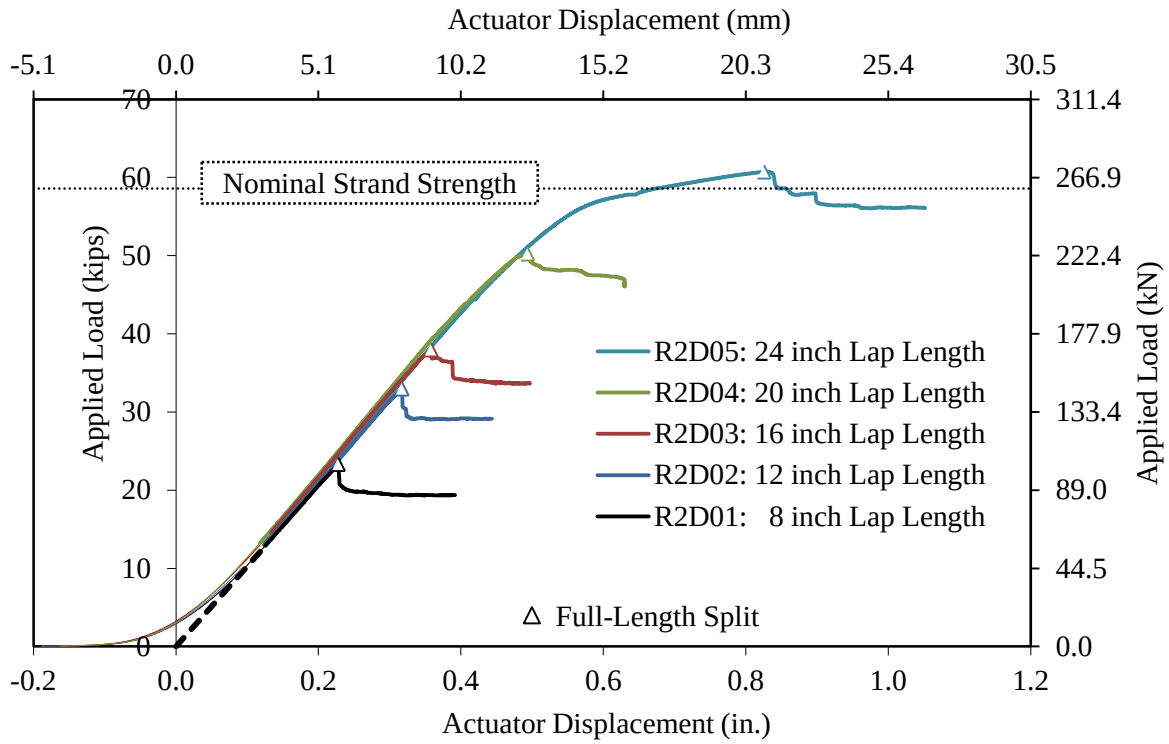

Figure 12. Graph. Load versus actuator displacement response for R2D specimens.

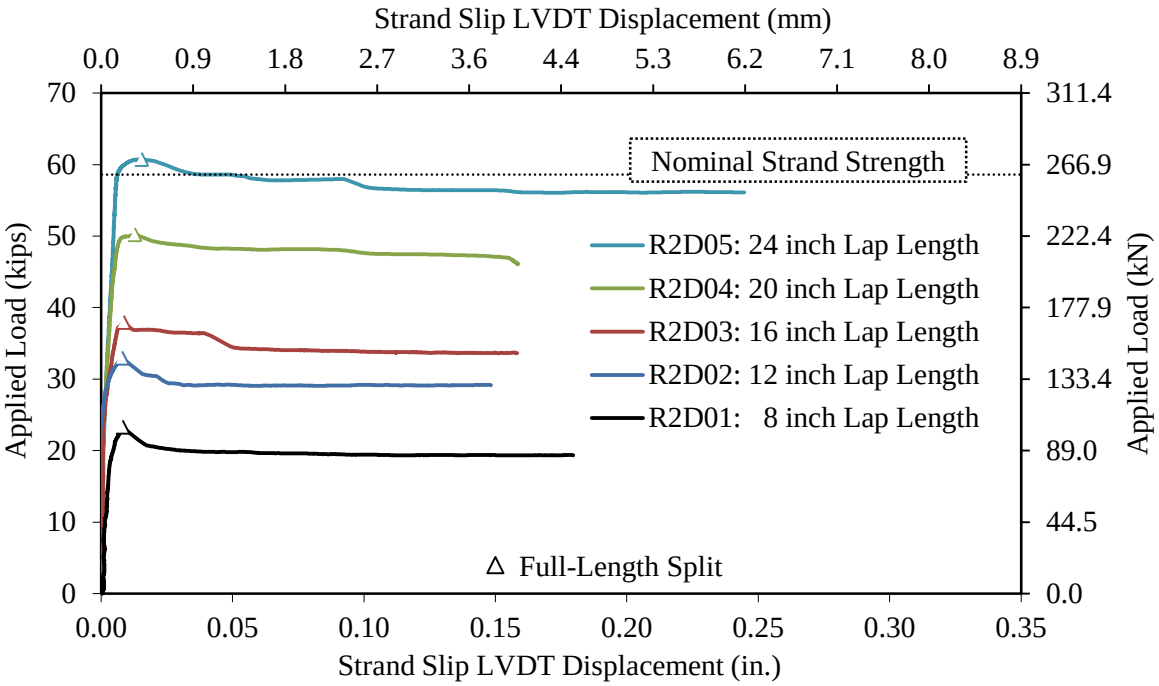

Figure 13. Graph. Load versus strand slip response for R2D specimens.

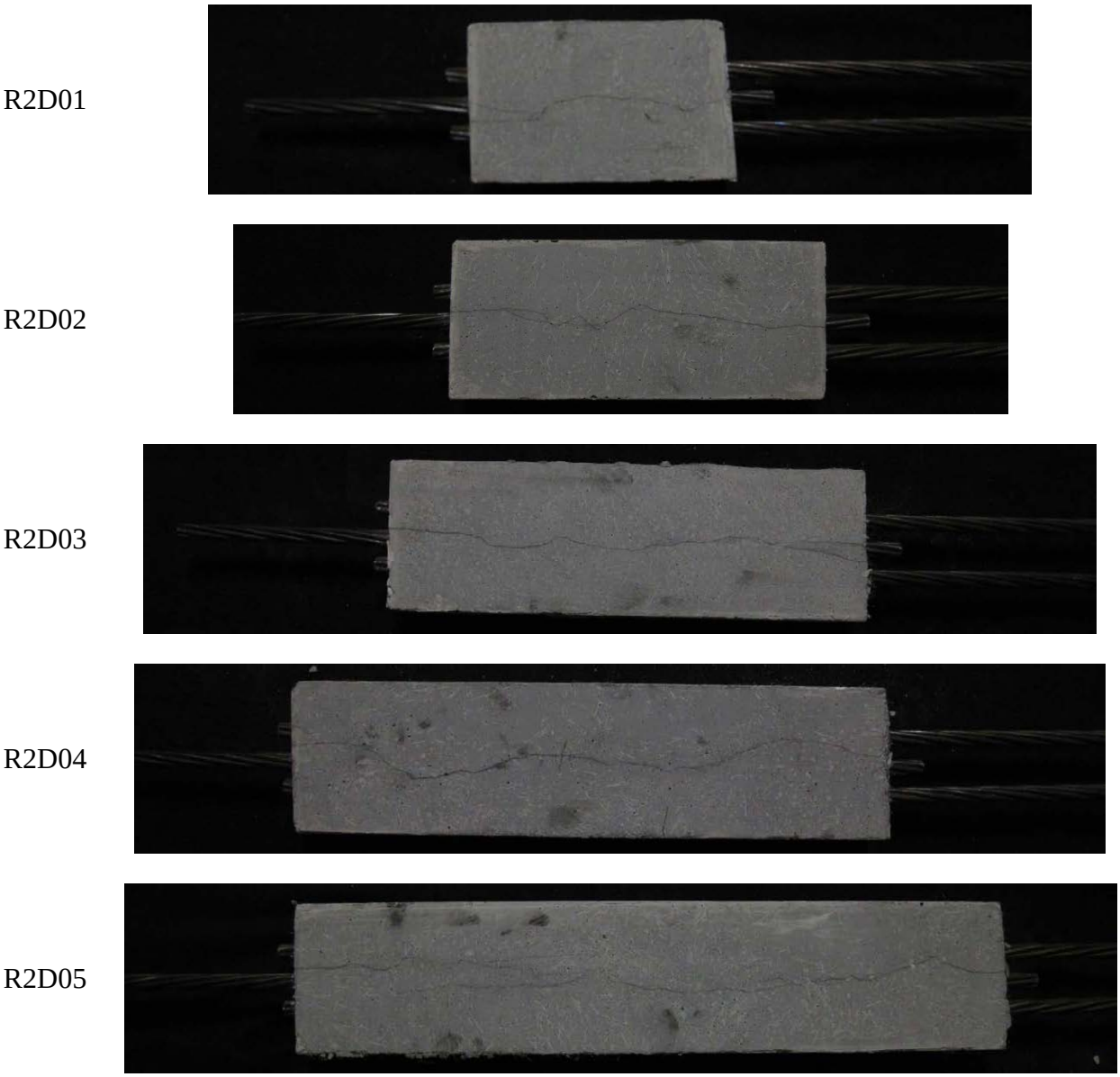

Figure 14. Photographs. Cracking apparent at conclusion of testing of R2D specimens.

Overall Strand Development Length

The strand pullout test results discussed in the previous section provide an indication of the strand splice length required for full development of the strand. The peak load achieved by each test specimen can be divided by the strand area to determine the peak strand stress achieved prior to strand slippage or rupture. These results are plotted in Figure 15 versus the length of each test specimen. The nominal strand strength of 270 ksi (1861 MPa) is also shown.

The R2A tests indicate that the non-contact lap splice length for a 0.5 inch (12.7 mm) strand in steel fiber reinforced UHPC is between 16 and 20 inches (0.4 and 0.5 m). A lap length less than 16 inches (0.4 m) may be possible if greater confinement is provided. The R2B and R2C tests indicate that the non-contact lap splice length for a 0.5 inch (12.7 mm) strand in PVA fiber reinforced UHPC is approximately 36 inches (0.91 m). Given that all of these specimens exhibited partial or full length splitting of the UHPC, increased confinement may allow for reduced lap lengths. The R2D tests indicate that the non-contact lap splice length for a 0.6 inch (15.2 mm) strand in steel fiber reinforced UHPC is approximately 24 inches (0.61 m). Again, increased confinement may allow for reduced lap lengths.

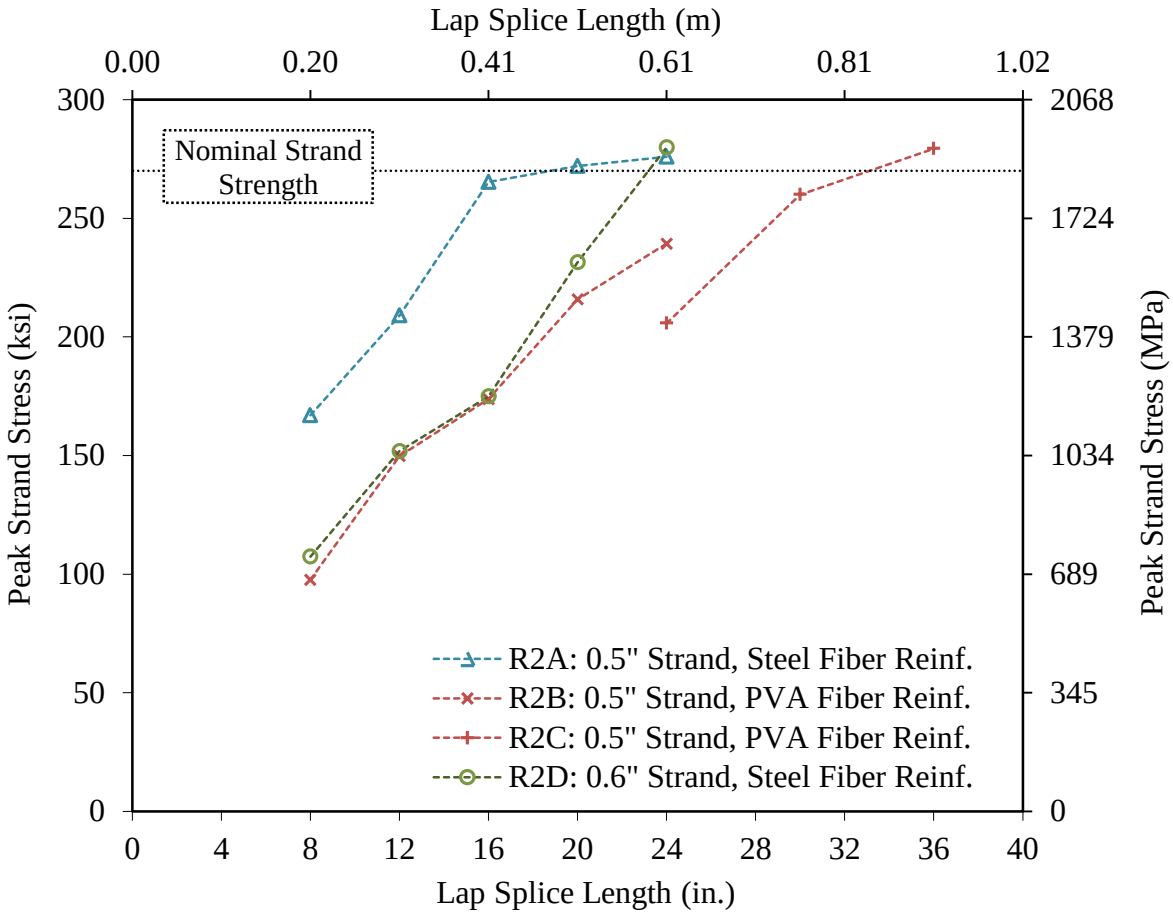

Figure 15. Graph. Peak strand stress versus lap splice length.

Research in the field of embedded element bond to concrete commonly normalizes the resistance to create a bond stress value. The equation in Figure 16 provides the relationship, wherein the applied load is divided by the bond length and the nominal circumference of the embedded element. The circumference of the seven-wire strand is taken as equal to the circumference of an equivalent diameter circle.

$$Bond\ Stress = \frac{Applied\ Load}{Bond\ Length \cdot \pi \cdot Strand\ Diameter}$$

Figure 16. Equation. Bond stress.

Using this equation and the development length summary discussed above, the average bond stress at peak load can be calculated. These values are plotted in Figure 17 for all specimens that exhibited slippage of strand at the peak load. The two R2A specimens that exhibited strand rupture are not plotted since their average bond stress at peak load was limited by the strength of the strand.

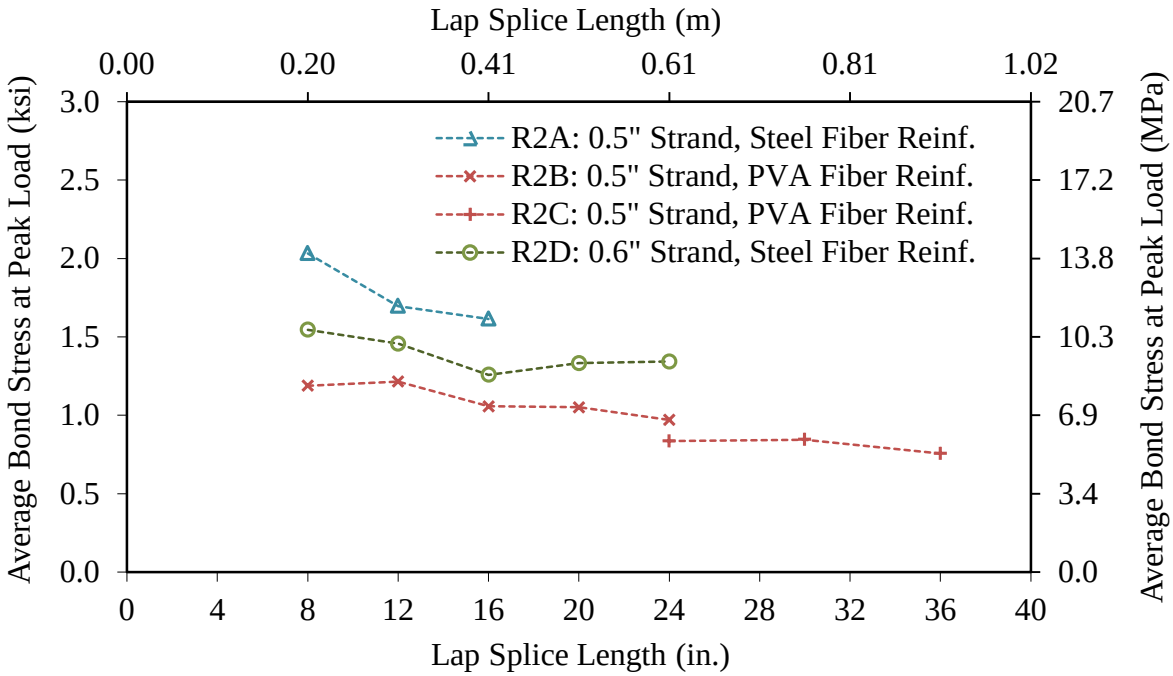

Figure 17. Graph. Average bond stress at peak load as a function of lap splice length.

These results demonstrate that the average bond stress at peak load decreases as the lap splice length increases. In practical terms, this behavior indicates that an increase in splice length will result in a less than proportional increase in the stress observed in the strand. For this reason, extrapolating bond stress results observed on particularly short specimens can result in an underestimation of the embedment length required for full development.

From the R2A tests with 0.5 inch (12.7 mm) strand in steel fiber reinforced UHPC, full development of the strand could occur with an average bond stress of approximately 1.6 ksi (11 MPa) over an 18 inch (0.46 m) lap splice length. From the R2B and R2C tests with 0.5 inch (12.7 mm) strand in PVA fiber reinforced UHPC, full development of the strands could occur with an average bond stress of approximately 0.75 ksi (5.2 MPa) over a 36 inch (0.91 m) lap splice length. From the R2D tests with 0.6 inch (15.2 mm) strand in steel fiber reinforced UHPC, full development of the strands could occur with an average bond stress of approximately 1.3 ksi (9 MPa) over a 24 inch (0.61 m) lap splice length. These values compare reasonably well with the results from Bertram and Hegger[8] wherein a high confinement, splitting restrained, steel fiber reinforced configuration at a load well below strand rupture was observed to generate a bond stress of approximately 1.9 ksi (13 MPa) over a short embedment length.

Overall Strand Sliding Friction Response

The post-peak load versus strand slip responses provide an indication of the sliding friction encountered by the single strand as it pulled out of the test specimen. The post-peak responses from all of the R2B, R2C, and R2D specimens as well as R2A01 and R2A02 were assessed to approximate the sliding friction as observed in terms of load per strand lap length. Table 7 provides the results of this assessment. The table also includes the calculated bond stress and an indication of whether the specimen exhibited a full-length splitting crack, a partial-length splitting crack, or did not exhibit a splitting crack.

In general terms, each set of test specimens provides an indication of the sliding friction response. In the R2A batch with 0.5 inch (12.7 mm) strand and steel fiber reinforcement, specimen R2A01 exhibited 3.1 kips/inch (0.55kN/mm) of sliding resistance equating to a bond stress of approximately 2.0 ksi (13.7 MPa). R2A02 exhibited 2.2 kips/inch (0.39 kN/mm) of sliding resistance equating to a bond stress of approximately 1.4 ksi (10 MPa). In the R2B and R2C batches with 0.5 inch (12.7 mm) strand and PVA fiber reinforcement, the specimens exhibited approximately 1.0 kips/inch (0.18 kN/mm) of sliding resistance. This equates to a bond stress of approximately 0.65 ksi (4.5 MPa). In the R2D batch with 0.6 inch (15.2 mm) strand and steel fiber reinforcement, the specimens exhibited approximately 2.4 kips/inch (0.42 kN/mm) of sliding resistance. This equates to a bond stress of approximately 1.3 ksi (9 MPa).

The higher sliding resistance values observed in the steel fiber reinforced specimens is likely due to the tighter cracks generally observed in steel fiber reinforced UHPC as compared to PVA fiber reinforced UHPC. The splitting cracks in the PVA fiber reinforced specimens in this study were observed to be significantly wider than the corresponding cracks in the steel fiber specimens. Tighter cracks correspond to greater confining stresses on the strand as it slides through the UHPC.

In total, these results provide an indirect indication of the lap splice length necessary to fully develop a strand in UHPC. Given that the pre-splitting sliding resistance will be greater than the post-splitting resistance, these values should provide a conservative indication of limiting bond stress and thus development length. Assuming that the confinement provided to the UHPC and/or the overall embedment length are sufficient to retard the development of a full length splitting crack, dividing the strand capacity by the post-peak sliding resistance should provide a conservative estimate of the full development length. For 0.5 inch (12.7 mm) strand in steel

fiber reinforced UHPC, this value would be approximately 18 inches (0.46 m) to reach the strand capacity of 41.3 kips (184 kN). For 0.6 inch (15.2 mm) strand in steel fiber reinforced UHPC, this value would be approximately 25 inches (0.64 m) to reach the strand capacity of 58.6 kips (261 kN). For 0.5 inch (12.7 mm) strand in PVA fiber reinforced UHPC, this value would be approximately 41 inches (1.0 m) to reach the strand capacity of 41.3 kips (184 kN).

Table 7. Strand sliding friction response.

Group	Specimen Name	Post-Peak Sustained Load			Full-Length Split	Partial-Length Split	No Split
		Load, kips (kN)	Load per Length, kips/in. (kN/mm)	Bond Stress, ksi (MPa)			
R2A	R2A01	25.4 (113)	3.2 (0.56)	2.02 (13.9)	X		
	R2A02	26.6 (118)	2.2 (0.39)	1.41 (9.7)	X		
	R2A03	N/A	N/A	N/A	X		
	R2A04	N/A	N/A	N/A			X
	R2A05	N/A	N/A	N/A			X
R2B	R2B01	9.1 (40)	1.14 (0.20)	0.72 (5.0)	X		
	R2B02	18.8 (84)	1.57 (0.27)	1.00 (6.9)	X		
	R2B03	17.8 (79)	1.11 (0.20)	0.71 (4.9)	X		
	R2B04	29.1 (129)	1.46 (0.26)	0.93 (6.4)	X		
	R2B05	30.3 (135)	1.26 (0.22)	0.80 (5.5)	X		
R2C	R2C01	21.9 (97)	0.91 (0.16)	0.58 (4.0)	X		
	R2C02	25.7 (114)	0.86 (0.15)	0.55 (3.8)	X		
	R2C03	34.1 (152)	0.95 (0.17)	0.60 (4.2)		X	
R2D	R2D01	20.0 (89)	2.50 (0.44)	1.33 (9.1)	X		
	R2D02	29.2 (130)	2.43 (0.43)	1.29 (8.9)	X		
	R2D03	36.5 (162)	2.28 (0.40)	1.21 (8.3)	X		
	R2D04	48.2 (214)	2.41 (0.42)	1.28 (8.8)	X		
	R2D05	58.7 (261)	2.45 (0.43)	1.30 (9.0)	X		

CHAPTER 5. CONCLUSIONS AND RECOMMENDATIONS

INTRODUCTION

The research discussed herein focused on assessing the development length of lap spliced prestressing strands in UHPC. Conclusions and proposed future research on this topic are presented in this chapter.

CONCLUSIONS

The following conclusions are presented based on the research presented in this report. The conclusions are divided into three sections. The first section focuses on material properties of the UHPC formulations tested in this study. The second focuses on the development length of prestressing strands in UHPC. The third section focuses on the test method implemented to assess the strand development length.

Material Properties

- The combined variations of fiber reinforcement type and mix design water content were observed to influence the compressive mechanical response of the tested UHPC formulations. The compressive strength and modulus of elasticity of the steel fiber reinforced batches were observed to be approximately 23.5 ksi (162 MPa) and 7400 ksi (51 GPa), respectively. For the PVA fiber reinforced batches with higher water content, these values were approximately 19 ksi (131 MPa) and 6800 ksi (47 GPa).
- The combined variations of fiber reinforcement type and mix design water content were observed to influence the density of the finished UHPC products. The density of the steel fiber reinforced batches was observed to be approximately 155 lb/ft^3 (2480 kg/m^3). For the PVA fiber reinforced batches with higher water content, the density was approximately 145 lb/ft^3 (2320 kg/m^3).

Strand Development Length

- The non-contact lap splice length required for development of prestressing strand in UHPC was significantly shorter than that anticipated for strands embedded in conventional concrete.
- Development of 0.5 inch (12.7 mm) diameter, 270-ksi (1860 MPa) prestressing strands can be achieved with a non-contact lap splice length of less than 20 inches (0.51 m) when embedded in steel fiber reinforced UHPC with a fiber reinforcement volumetric ratio of 2 percent. Development in 16 inches (0.4 m) or less may be possible if greater confinement is provided.
- Development of 0.6 inch (15.2 mm) diameter, 270-ksi (1860 MPa) prestressing strands can be achieved with a non-contact lap splice length of approximately 24 inches (0.61 m) when embedded in steel fiber reinforced UHPC with a fiber reinforcement volumetric ratio of 2 percent. A shorter lap splice length may be possible if greater confinement is provided.

- Development of 0.5 inch (12.7 mm) diameter, 270-ksi (1860 MPa) prestressing strands can be achieved with a non-contact lap splice length of approximately 36 inches (0.91 m) when embedded in PVA fiber reinforced UHPC with a fiber reinforcement volumetric ratio of 2 percent. A shorter lap splice length may be possible if greater confinement is provided.

Development Length Test Method

- The direct tension strand lap splice test method developed and implemented herein accurately replicates strand splice conditions that may exist in practice and thus affords a good model for assessing the bond performance of lap spliced strands.
- The test setup and testing procedure can be replicated by other research and testing organizations. They require no specialized equipment beyond a uniaxial tensile testing machine with servo-hydraulic displacement control and appropriate loading fixtures.
- Given the short development length afforded by some UHPC formulations, the implemented test method may be a simple, consistent method for assessing bond of reinforcements embedded in UHPC. Traditional concentric pullout tests, although simple to conduct, introduce an unrealistic stress state around the embedded element. Beam end pullout tests require a more complex test setup and larger test specimens.

FUTURE RESEARCH

This study both developed and implemented a test method to assess the development length of untensioned prestressing strands embedded in UHPC. Future research on this topic to investigate different UHPC paste formulations, UHPC fiber reinforcements, strand sizes, cover distances, and supplemental confinement configurations is warranted.

Research to develop and test structural connections with lap-spliced prestressing strands is also warranted.

ACKNOWLEDGMENTS

The research which is the subject of this document was funded by the U.S. Federal Highway Administration. This support is gratefully acknowledged.

This research project could not have been completed were it not for the dedicated support of the federal and contract staff associated with the FHWA Structural Concrete Research Program. Special recognition goes to Gary Greene formerly of PSI, Inc. who assisted with the scoping of the project, the specimen design, and the test setup. Recognition also goes to Carmelo Di Bella and Daniel Balcha who provided technical support throughout the casting and preparation of the test specimens. Carmelo and Daniel were employed by Global Consulting, Inc. at TFHRC under contract DTFH61-07-C-00011 at the time of the testing discussed herein. Gary was employed at TFHRC under contract DTFH61-10-D-00017.

The publication of this report does not necessarily indicate approval or endorsement of the findings, opinions, conclusions, or recommendations either inferred or specifically expressed herein by the Federal Highway Administration or the United States Government.

REFERENCES

1. Graybeal, B., "Ultra-High Performance Concrete," U.S. Department of Transportation, Federal Highway Administration, FHWA-HRT-11-038, March 2011, 8 pp.

2. Graybeal, B., "Construction of Field-Cast Ultra-High Performance Concrete Connections," U.S. Department of Transportation, Federal Highway Administration, FHWA-HRT-12-038, April 2012, 8 pp.

3. Graybeal, B., "Material Property Characterization of Ultra-High Performance Concrete," Federal Highway Administration, Report No. FHWA-HRT-06-103, August 2006, 186 pp.

4. Castrodale, R. and C. White, "Extending Span Ranges of Precast Prestressed Concrete Girders," NCHRP Report 517, National Cooperative Highway Research Program, Transportation Research Board, 2004, 603 pp.

5. Parker, A., M. Hueste, and J. Mander, "Continuous Precast, Prestressed Concrete Girder Bridge Systems," Proceedings, 2012 Transportation Research Board Annual Meeting, January 2012, 15 pp.

6. Salmons, J., and T. McCrate, "Bond Characteristics of Untensioned Prestressing Strand," *PCI Journal*, V. 22, No. 1, January-February 1977, pp. 52-65.

7. Chao, S-H., A. Naaman, and G. Parra-Montesinos, "Bond Behavior of Strand Embedded in Fiber Reinforced Cementitious Composites," *PCI Journal*, V. 51, No. 6, November-December 2006, pp. 56-71.

8. Bertram, G., and J. Hegger, "Bond Behavior of Strands in UHPC – Tests and Design," *Proc. 3rd International Symposium on UHPC*, Kassel, Germany, March 2012, pp. 525-532.

9. ASTM C39-11, "Standard Test Method for Compressive Strength of Cylindrical Concrete Specimens," *ASTM Book of Standards Volume 04.02*, ASTM International, West Conshohocken, PA, 2011.

10. ASTM C469-10, "Standard Test Method for Static Modulus of Elasticity and Poisson's Ratio of Concrete in Compression," *ASTM Book of Standards Volume 04.02*, ASTM International, West Conshohocken, PA, 2010.

11. Graybeal, B.A., 2007, "Compressive Behavior of Ultra-High Performance Fiber-Reinforced Concrete," *ACI Materials Journal*, V. 104, No. 2, Mar.-Apr., pp. 146-152.

12. Graybeal, B., and B. Stone, "Compression Response of a Rapid-Strengthening Ultra-High Performance Concrete Formulation," Federal Highway Administration, National Technical Information Service Accession No. PB2012-112545, September 2012, 66 pp.